Linear viscoelasticity of bio-based composites of polylactic acid and regenerated cellulose fibers: modeling and experimental validation

Yu Chen[a], Tian Tang[a,*], Cagri Ayranci[a,*]

[a.] *Department of Mechanical Engineering, University of Alberta, Edmonton, Alberta, T6G 1H9, Canada*

[*]corresponding co-authors

Abstract

A viscoelastic constitutive relationship of bio-based composites made from polylactic acid (PLA) and regenerated cellulose fibers (RCF) is developed by extending the Halpin-Tsai-Pagano model for linear elastic composites to the linear viscoelastic regime using the correspondence principle. To predict the creep compliance of PLA/RCF composites, the model only requires the constitutive relationships of the constituents, as well as concentration and geometry of the RCF. PLA/RCF composites with different RCF concentration are manufactured using a customized core-shell extrusion process, and creep tests are performed to extract their creep compliances. Good agreement is found between the model prediction and experimental results. The model has the potential to predict the linear viscoelasticity of other types of bio-based composites reinforced by short fibers.

Keywords: biocomposite, creep, analytical modeling, extrusion.

1 Introduction

Since the 1990s, the use of traditional petroleum-based fiber-reinforced polymeric composites have been critically discussed mainly due to increased environmental concerns [1]. Examples include polymers such as polystyrene (PS) and polyethylene terephthalate (PET)

reinforced by fibers such as glass, aramid or carbon. The concept of bio-based composites has been proposed as an alternative [2]. Bio-based composites are composites made from bio-renewable and bio-degradable constituents [2]. In recent years, these bio-based composites have started to be widely used in large-volume industries, such as automotive and construction. For example, the major car manufacturers in Germany (Mercedes, BMW, Volkswagen Audi groups) are now making interior trim components such as dashboards and door panels, using bio-based composites [2,3]. In the construction industry, bio-based composites have been used to manufacture doors, side panels, roofing sheets, etc. [2].

For the matrix phase of bio-based composites, polylactic acid (PLA), polyglycolic acid (PGA), poly(3-hydroxybutyrate-co-3-hydroxyvalerate) (PHBV), poly(butylene succinate) (PBS) and thermoplastic starch have been reported to become alternatives to petroleum-based polymers [4]. Among these, PLA is becoming increasingly popular due to a variety of reasons [5]. Firstly, PLA can be derived from some of the abundant types of bio-renewable resources such as corn starch and sugar cane and that leads to large-scale production capacity [6]. Secondly, the stiffness of PLA is comparable to petroleum-based polymers such as PS and PET [7]. Thirdly, PLA is a semi-crystalline thermoplastic which can be processed using well-established melt-processing techniques such as extrusion, injection molding and compression molding. [6]. Finally, PLA is environment-friendly [6], and can be reused, recycled or biodegraded under both natural and controlled environments [8].

For the reinforcement phase of bio-based composites, natural fibers have various advantages over synthetic fibers [9], including renewability, biodegradability, cost effectiveness, low density, etc. [1,2]. Cellulose-based plant fibers such as jute, flax, hemp and kenaf are

frequently used natural fibers, due to their moderate price, high availability, and good mechanical properties [2]. Studies have shown that the incorporation of these cellulose-based plant fibers into PLA can increase its modulus, enhance the toughness, and improve the thermal stability [10–12]. The reinforcements can even promote the biodegradation of PLA due to their high hydrophilicity, which enhances moisture adsorption and hydrolytic degradation of PLA [13]. However, the major drawbacks of natural fibers are their inconsistency and the impurities on the fiber surface [5]. Mechanical properties of natural fibers can vary significantly among different batches, and surface impurities such as wax, pectin, hemicellulose and lignin can greatly affect the adhesion between the natural fibers and PLA matrix [14]. For this reason, emerging studies have shown interests in reinforcing PLA with regenerated cellulose fibers (RCF) [15–20]. RCF are generated from cellulose separated from bio-feedstock using various chemical processes [21]. For instance, Lyocell fibers are extracted from wood chips by dissolving them in non-toxic N-Methyl morpholine N-oxide (NMMO) and pumping them through the spinnerets into coagulation baths where regeneration of the cellulose takes place [21]. This is an environmentally friendly process since 99% of the NMMO solvent can be recovered and reused [22]. Compared with natural fibers, RCF have better consistency, improved mechanical properties and almost no surface impurities since the fiber surface have been cleaned during extraction [14,23]. PLA/RCF bio-based composites have the potential to replace petroleum-based non-biodegradable polymer composites or offer excellent alternatives, in a wide range of applications such as boxes for packaging, beams for decking and door panels for automotives [24].

A number of investigations have been carried out to study the manufacturing and characterization of PLA/RCF bio-based composites. Melt-mixing is the most frequently used

method for embedding RCF into PLA matrix, while injection molding and compression molding have also been attempted[5,14,23,24]. In characterizing the mechanical properties of PLA/RCF composites, Bledzki et al. [14] discovered that the addition of 30 wt% RCF increased the Young's modulus by approximately a factor of 1.7 in comparison to bare PLA [14]. Besides Young's modulus, Bax and Mussig [25] reported a significant increase in tensile strength and Charpy impact strength with the addition of 10-30 wt% RCF. Thermo-mechanical properties characterized by dynamic mechanical analysis were also reported in the literature. Huda et al.[23], Baghaei et al. [18], Zhang et al. [26] and Kurokawa et al. [7] all reported an increased storage modulus when RCF were added into PLA, regardless of the manufacturing method. These findings suggest good compatibility between RCF and PLA, which enables effective stress transfer on the fiber-matrix interface. Furthermore, Baghaei et al. [18], Zhang et al. [26] and Kurokawa et al. [7] reported a drastic increase in storage modulus above PLA's glass transition temperature, suggesting that the thermal stability and heat resistance of PLA has been significantly enhanced by the reinforcement of RCF.

Despite the enthusiasms in manufacturing and charactering PLA/RCF bio-based composites, attempts to model their mechanical properties have been limited [23,24,27,28]. Huda et al. [23] provided a linear fitting to describe the increasing tensile modulus of the composite with respect to RCF content. Ganster et al. [27] and Rozite et al. [24] applied modified rule of mixture to predict the Young's modulus E_c of PLA/RCF composites:

$$E_c = \eta_l \eta_\theta E_f V_f + E_m V_m \quad (1)$$

where E_f and E_m are the Young's moduli of RCF and PLA, respectively; and V_f and V_m are volume fraction of RCF and PLA, respectively. η_l and η_θ are two empirical parameters

introduced to capture the effect of fiber length and orientation on E_c, which do not have direct physical meaning and need to be extracted from fitting to experimental data. Karakoc et al. [28] used high-resolution X-ray microcomputed tomography (Micro-CT) to characterize the internal structure of a PLA/RCF bio-based composite sample and incorporated it into a finite element solver to simulate its mechanical behavior under different loadings. Effective elastic properties were determined from the simulation results. However, the above-mentioned work by Karakoc et al. [28] still assumed the composite to be elastic while PLA has been discovered to exhibit viscoelasticity [29]. Consequently, the PLA/RCF composites can show viscoelastic behaviors such as creep and stress relaxation [30], which may impact the performance of the composites under long-term loadings. To the best of the authors' knowledge, only Rozite et al. [24] conducted creep-recovery tests on PLA/RCF composites, with 5 wt% RCF reinforcement. The composites were found to exhibit creep behavior similar to conventional polymer-based composites [24]. Our literature search did not render predictive models capable of capturing the viscoelasticity of PLA/RCF composites, indicating an important gap in the literature.

Consequently, the present work aims at developing a constitutive model that can accurately describe the viscoelastic behavior of PLA/RCF bio-based composites, while being simple enough for usage by a broad audience. In the literature, a variety of models has been proposed and validated to predict the elastic constitutive relation of fiber reinforced polymer composites with different assembly structures [31]. For instance, Vilaseca et al. [32] proposed a model that combines the Tsai-Pagano model [33] and Halpin-Tsai model [34], which predicts the Young's modulus of short fiber reinforced polymer composites based on fiber morphology, fiber distribution, as well as mechanical properties of the fiber and matrix. Mazzanti et al. [35] applied this model to PLA bio-based composites reinforced by alkali treated hemp fibers and found good

agreement with experiments for hemp concentration up to 6 wt%. In this work, we go beyond the linear elastic regime and develop a model that predicts the creep compliance of PLA/RCF bio-based composites. Validated against experimental results, the developed model has the potential to predict the linear viscoelasticity of other types of bio-based composites reinforced by short fibers.

2 Model

Consider a PLA/RCF composite where the RCF are homogeneously distributed with random orientation in the PLA matrix. The bonding between fiber and matrix is assumed to be perfect with no interfacial defects. Widely used in a variety of applications, this type of composite can be considered as a statistically homogeneous and isotropic material [36]. The focus of the modeling is to derive the time (t) dependent creep compliance $J_c(t)$ of the composite in the linear viscoelastic regime. Under one-dimensional loading, the stress $\sigma_c(t)$ and strain $\varepsilon_c(t)$ of the composite are related through $J_c(t)$, given by [37]

$$\varepsilon_c(t) = \int_0^t J_c(t-\tau) d\sigma_c(\tau). \quad (2)$$

In linear viscoelasticity, it is a common approach to determine the creep compliance or stress relaxation function in one-dimensional form [38], which can then be extended to higher dimensions [31,34]. Below we will first formulate the constitutive relations for the constituents (RCF, PLA), after which $J_c(t)$ will be derived based on a homogenization approach coupled with the correspondence principle.

2.1 Constitutive relations for the constituents

RCF are usually highly crystallized [39]; it is therefore reasonable to assume the RCF reinforcement in the composite to be linearly elastic, satisfying the following constitutive relation

$$\sigma_f(t) = E_f\,\varepsilon_f(t), \qquad \text{or} \qquad \varepsilon_f(t) = S_f\sigma_f(t) \tag{3}$$

where $\sigma_f(t)$ and $\varepsilon_f(t)$ are the stress and strain of the RCF, respectively. E_f and S_f are the Young's modulus and elastic compliance of the fibers respectively, which are time-independent and related by $E_f S_f = 1$. A previous study by our group [29] showed that PLA exhibits linear viscoelasticity, which can be described by the Burgers model as schematically shown in Figure 1 (a). E_{m1} and E_{m2} are elastic constants of the linear Hookean springs, and μ_{m1} and μ_{m2} are viscosities of the linear viscous dashpots. $\sigma_m(t)$ and $\varepsilon_m(t)$ are the stress and strain of PLA, respectively [38]. The creep compliance for this model is given by [38]

$$J_m(t) = \frac{1}{\mu_{m2}}t + \frac{1}{E_{m2}} + \frac{1}{E_{m1}}\left[1 - \exp\left(-\frac{E_{m1}}{\mu_{m1}}t\right)\right] \tag{4}$$

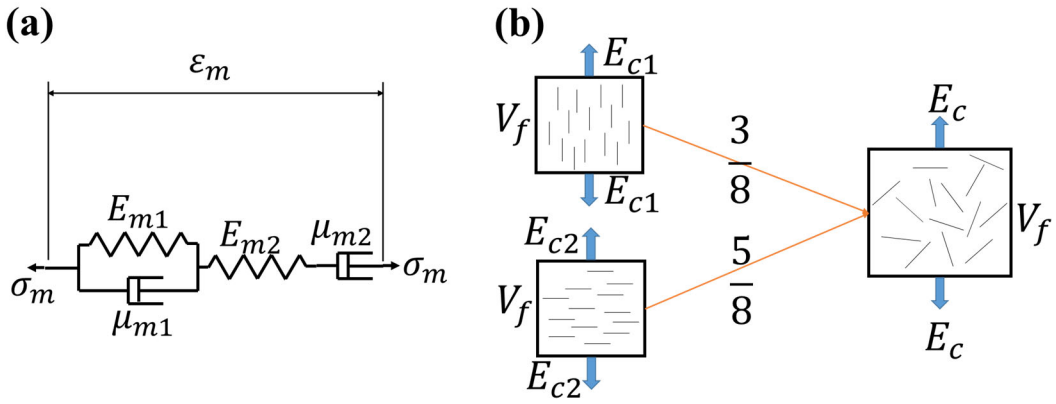

Figure 1. Schematic representation of (a) linear Burgers model for PLA [38]; (b) Tsai-Pagano model for linear elastic composites [33].

2.2 Composite model

Since the constitutive relations of both constituents follow linearity, the correspondence principle can be used to extend a linear elastic model to the corresponding linear viscoelastic model in the Laplace transformed domain [30,37,40]. Tsai and Pagano [33] proposed a linear elastic model for composites reinforced by homogeneously distributed and randomly oriented fibers. The effective Young's modulus (E_c) of the composite is calculated by the weighted average of the longitudinal (E_{c1}) and transverse (E_{c2}) Young's moduli of composites reinforced by aligned short fibers with the same volume fraction (V_f). This relation is given by equation (5) and schematically depicted in Figure 1 (b).

$$E_c = \frac{3}{8}E_{c1} + \frac{5}{8}E_{c2} \tag{5}$$

E_{c1} and E_{c2} can be determined by the Halpin-Tsai model [34,41,42]

$$\frac{E_{ci}}{E_m} = \frac{1 + \xi_i \eta_i V_f}{1 - \eta_i V_f}, \qquad \eta_i = \frac{E_f/E_m - 1}{E_f/E_m + \xi_i} \tag{6}$$

where E_m and E_f are the Young's moduli of matrix and fiber respectively; $i\ (= 1, 2)$ indicates the direction; ξ_i is a semi-empirical parameter related to the fiber aspect ratio and the direction i. Halpin and Kardos [34] provided the values of ξ_i for aligned short fiber reinforced composites. In the longitudinal direction ($i = 1$), $\xi_1 = 2L_f/d_f$, where L_f and d_f are respectively the length and diameter of the reinforcement fibers. In the transverse direction ($i = 2$), $\xi_2 = 2$.

Defining the elastic compliance to be the reciprocal of Young's modulus ($S_m = 1/E_m$, $S_f = 1/E_f$, $S_c = 1/E_c$, $S_{c1} = 1/E_{c1}$, $S_{c2} = 1/E_{c2}$), equations (5) can also be written into

$$\frac{1}{S_c} = \frac{3}{8}\frac{1}{S_{c1}} + \frac{5}{8}\frac{1}{S_{c2}} \tag{7}$$

where the elastic compliances in the longitudinal and transverse directions, S_{ci} $(i = 1,2)$, are obtained from equation (6) and given by

$$\frac{1}{S_{ci}} = \frac{1}{S_m}\frac{1+\xi_i\eta_i V_f}{1-\eta_i V_f}, \qquad \eta_i = \frac{S_m/S_f - 1}{S_m/S_f + \xi_i} \tag{8}$$

The above elastic solution can now be extended into the linear viscoelastic regime using the correspondence principle. Denote the Laplace transformed creep compliances of the matrix, the fiber and the composite by $\hat{J}_m(s)$, $\hat{J}_f(s)$ and $\hat{J}_c(s)$ respectively, where s is the independent variable in the Laplace domain. $\hat{J}_m(s)$ and $\hat{J}_f(s)$ can be obtained by taking the Laplace transform $\mathcal{L}\{\bullet\}$ of equation (4) and the constant fiber compliance S_f, leading to

$$\hat{J}_m(s) = \mathcal{L}\{J_m(t)\} = \frac{1}{\mu_{m2}\, s^2} + \frac{1}{E_{m2}\, s} + \frac{1}{E_{m1}\, s + \mu_{m1}\, s^2} \tag{9}$$

$$\hat{J}_f(s) = \mathcal{L}\{J_f(t) = S_f\} = \frac{S_f}{s} \tag{10}$$

Based on the correspondence principle [30], the Laplace transformed creep compliances of the linear viscoelastic composite follow the same relationship, equation (7), for the compliances of the linear elastic composite, i.e.,

$$\frac{1}{s\hat{J}_c(s)} = \frac{3}{8}\frac{1}{s\hat{J}_{c1}(s)} + \frac{5}{8}\frac{1}{s\hat{J}_{c2}(s)} \tag{11}$$

where

$$\frac{1}{s\hat{J}_{ci}(s)} = \frac{1}{s\hat{J}_m(s)}\frac{1+\xi_i\eta_i V_f}{1-\eta_i V_f}, \qquad \eta_i = \frac{[s\hat{J}_m(s)]/[s\hat{J}_f(s)] - 1}{[s\hat{J}_m(s)]/[s\hat{J}_f(s)] + \xi_i} \qquad i = 1,2 \tag{12}$$

are extended from the elastic solution, equation (8). Combining equations (9), (10), (11) and (12), $\hat{J}_c(s)$ is calculated to be

$$\hat{J}_c(s) = \frac{F_6 s^6 + F_5 s^5 + F_4 s^4 + F_3 s^3 + F_2 s^2 + F_1 s + F_0}{D_7 s^7 + D_6 s^6 + D_5 s^5 + D_4 s^4 + D_3 s^3 + D_2 s^2} \quad (13)$$

where F_j (j = 0 to 6) and D_k (k = 2 to 7) are constants related to E_{m1}, E_{m2}, μ_{m1}, μ_{m2}, E_f, ξ_1 and ξ_2, as given in the supplementary information. The creep compliance of the composite in the time domain, $J_c(t)$, is finally obtained by taking the inverse Laplace transform of $\hat{J}_c(s)$

$$J_c(t) = \mathcal{L}^{-1}\{\hat{J}_c(s)\} \quad (14)$$

The full expression of $J_c(t)$ was obtained using the symbolic core of Mathematica® (Wolfram Research, USA). It is lengthy (involving over 3000 terms) and therefore not presented here.

3 Experiments

3.1 Materials

Extrusion grade PLA (4043D) was obtained from NatureWorks LLC, USA. Its number-average molecular weight (M_n) is 106,000 g/mol, and it has a D-lactic acid content of 4.5 to 5 wt% [43]. The RCF used in this work was BioMid®, obtained from Gordon Shank Consulting and Engineered Natural Composites, Inc., Canada. These BioMid® fibers are continuous strands of RCF made from the wastes generated during lumber production in western Canada [44]. It has been reported that BioMid® fibers has a crystallinity of 95% and it can sustain a processing temperature of 360°C, which is higher than the majority of the natural fibers [45,46].

3.2 Composite Manufacturing

Attempts were made to chop the long continuous RCF into short fibers and melt-mix it with PLA. However, good dispersion of RCF in PLA was not possible due to the limitation of the single screw extruder in our laboratory. Thus, the following unconventional two-step extrusion technique was utilized to produce PLA/RCF composites.

3.2.1 Masterbatch preparation

Both PLA and RCF fibers were dried under vacuum at 80°C for 8 h in a Lindberg/Blue M™ vacuum oven (Thermo Fisher Scientific, USA) to remove the residual moisture that may cause air bubbles during extrusion. Then, a Brabender™ single screw extruder equipped with a core-shell die (a.k.a. crosshead die), attached to an ATR Plasti-Corder drive system (C.W. Brabender Instruments, Inc., Germany), was used to manufacture the masterbatch of the PLA/RCF composites containing 5.6 wt% RCF. The extrusion process is schematically shown in Figure 2 (a) and the cross-sectional view of the core-shell die is shown in Figure 2 (b). In this process, the long continuous RCF strand went through the core part of the die while the PLA pellets were melted in the extruder and flow through the shell part of the die. The processing temperature and screw speed (in RPM) for the masterbatch preparation are shown in the table in Figure 2 (a), which were selected based on the manufacturer provided data for 4043D PLA pellets. Finally, the extrudate was cooled by Filabot™ FB00626 cooling fan (Triex LLC, USA) with 100% fan level and Filabot™ FB00073 filament spooler (Triex LLC, USA) was used to pull the 5.6 wt% PLA/RCF composite masterbatch. Attempts were made to increase the fiber concentration; however, significant agglomeration of RCF was observed. Pure PLA masterbatch filaments without RCF reinforcement were also produced using the same extrusion setup and processing parameters.

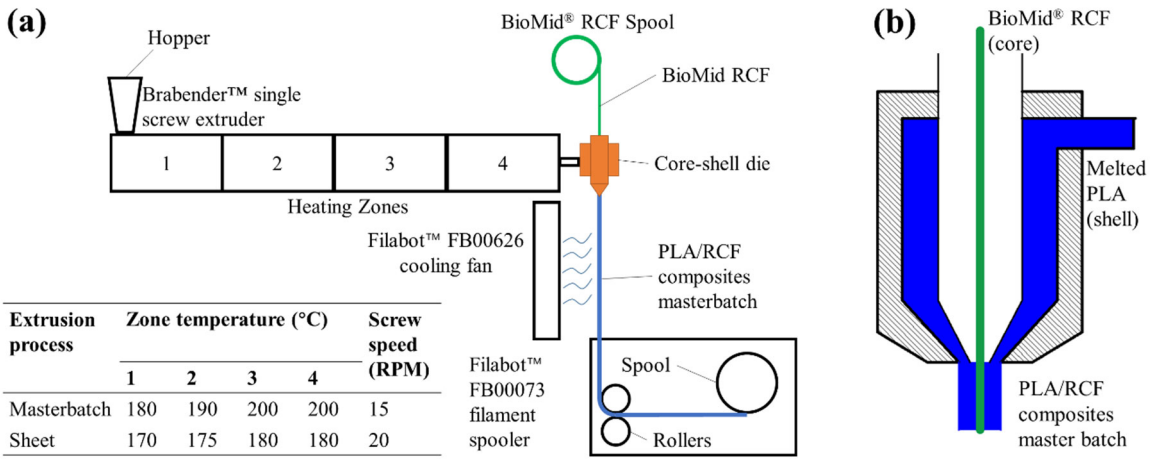

Extrusion process	Zone temperature (°C)				Screw speed (RPM)
	1	2	3	4	
Masterbatch	180	190	200	200	15
Sheet	170	175	180	180	20

Figure 2. (a) Schematic representation of the core-shell extrusion process and the processing parameters. (b) Schematics for the cross-section of the core-shell die shown with orange in (a).

3.2.2 Sheet sample preparation

Both masterbatches (pure PLA and 5.6 wt% PLA/RCF composite) were chopped into pellets and the prepared composite pellets are shown in Figure 3 (a). These pellets were again dried under vacuum at 80°C for 8 h in the Lindberg/Blue M™ vacuum oven to remove the residual moisture. Then, the Brabender™ single screw extruder was used with a fixed sheet die (100 mm in width and 0.5 mm in thickness) to produce sheet samples. The processing parameters for the sheet preparation stage were slightly different from the masterbatch preparation stage (Figure 2 (a)) to minimize excessive shrinkage during cooling.

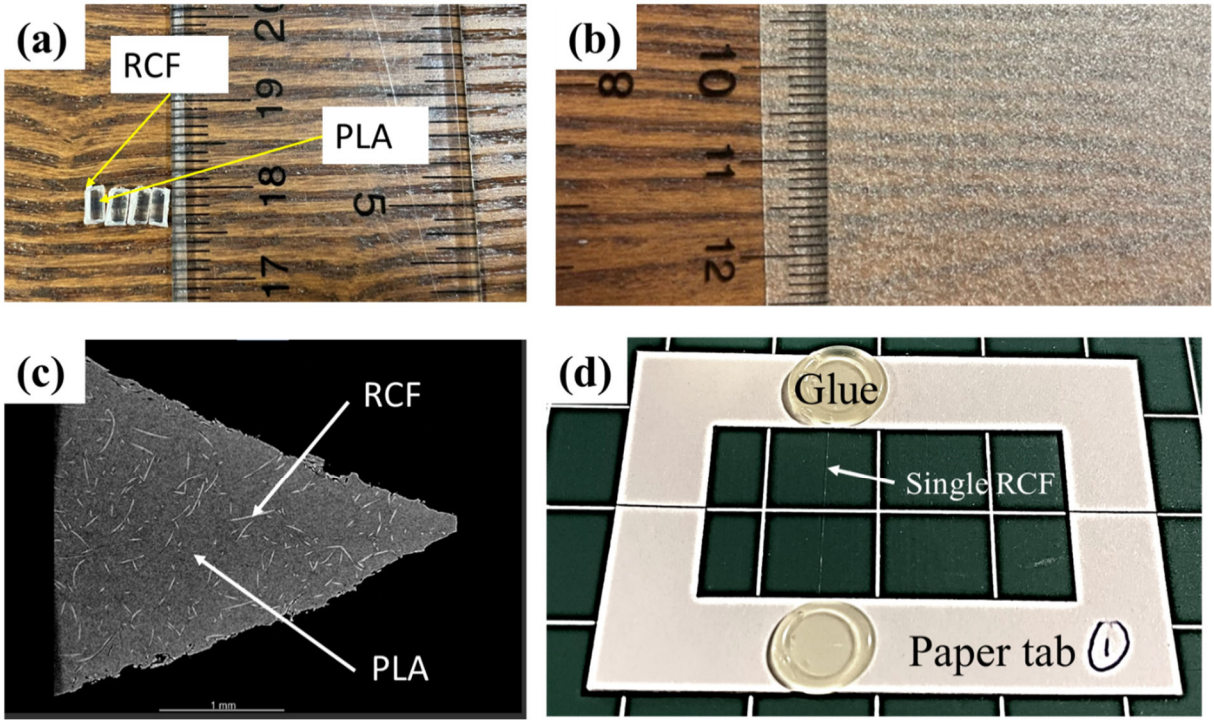

Figure 3. (a) Chopped masterbatch pellets; the gaps on the ruler are 1 mm; (b) A sheet sample of 5.6PLA/RCF; (c) Micro-CT image of a triangular section of a sheet sample of 5.6PLA/RCF; (d) Mounting of the single RCF for tensile tests (sharpness was tuned to better visualize the sample)

Sheet samples with three different RCF concentrations were produced. Pure PLA samples (0.0PLA/RCF) were produced using pure PLA masterbatch; 2.8 wt% RCF reinforced PLA composites (2.8PLA/RCF) were produced by diluting the 5.6 wt% PLA/RCF masterbatch with pure PLA masterbatch at 1:1 ratio; 5.6 wt% RCF reinforced PLA/RCF composites (5.6PLA/RCF) were produced using the 5.6 wt% PLA/RCF masterbatch. Due to the shear force provided during the extrusion, the fibers were approximately homogeneously distributed and randomly oriented in the sheet samples, as shown in Figure 3 (b). In order to confirm the random orientation of RCF, Micro-CT characterization was performed on a triangular section of a 5.6PLA/RCF sample as shown in Figure 3 (c). The histogram of fiber orientation is presented in

the supplementary information, which deviates slightly from a uniform distribution. This suggests that there is still some non-ideality for dispersing the RCF in the composite using the two-step extrusion process.

3.3 Characterization

3.3.1 Parameters of RCF

RCF bundles were separated by hand into single RCF samples and their diameters (d_f) were measured with calibrated Olympus IX-83 confocal microscope (Olympus Corporation, Japan). A total of 80 measurements were taken for d_f. To determine the fiber length (L_f) in the produced composites, it was assumed that L_f did not change during the sheet sample extrusion process. Therefore L_f was measured from the length of chopped pellets shown in Figure 3 (a). A total of 100 measurements for L_f were taken.

Tensile tests were conducted to measure the Young's modulus (E_f) of single RCF according to ASTM D3379 [47]. A universal tensile testing system (ElectroForce 3200 Series III, Bose Corporation, USA) equipped with a 250 g load cell was used. As shown in Figure 3 (d), the single RCF was mounted by hand onto a paper tab by poly(ethylene-vinyl acetate) (PEVA, marked as "glue" in the figure) using a glue gun (Topelek, China). The gauge length of the paper tab was 20 mm. After mounting the sample on the tensile clamps, the paper tab was cut, and a constant displacement rate of 0.6 mm/min was applied [47]. The ambient environment during the tests was 18% RH and around 22°C. The nominal stress was calculated using the measured diameter d_f as described above. The Young's modulus was determined by linear fitting of the initial part of the stress-strain curve. Ten RCF samples were tested to obtain the averaged Young's modulus.

3.3.2 Creep tests

Sheet samples (0.0PLA/RCF, 2.8PLA/RCF and 5.6PLA/RCF) were cut into rectangles of 60 mm long and 10 mm wide to be mounted onto the tensile clamps of the aforementioned universal tensile testing system. The samples were dried under vacuum at 80°C for 8 h in the Lindberg/Blue M™ vacuum oven to remove the moisture and release the residual stress that might have been generated during the extrusion process. Tensile creep tests were then conducted on each sample for 15 min following ASTM D2990 [48], where the creep stress was programmed to be applied within 1 s and the strain was recorded every 50 s. A series of pre-tests were first conducted with different creep stresses σ_0 to identify the linear viscoelastic limit. The measured strain was normalized by σ_0 to obtain the creep compliance. According to the results of these pre-tests, the creep compliance did not change with σ_0 when $\sigma_0 \leq 6.8$ MPa, regardless of the RCF concentration. Thus, 6.8 MPa was used as the stress for all creep tests. Five replications were performed at each RCF concentration. The ambient environment during creep tests was around 22% RH and 23°C.

3.3.3 Crystallinity of PLA matrix

Differential scanning calorimetry (DSC) measurements were conducted on DSC Q100 (TA instruments, USA) in the temperature range of 20-180°C for 0.0PLA/RCF, 2.8PLA/RCF and 5.6PLA/RCF to measure the crystallinity of the PLA matrix [12]. The heating scan was performed with a heating rate of 5°C/min. The crystallinity X_c of PLA in the samples was calculated by [49]

$$X_c = \frac{\Delta H_m - \Delta H_c}{\Delta H_{mf}} \times 100\% \quad (15)$$

where ΔH_m is the heat of fusion, ΔH_c is the heat of crystallization during the DSC scan, and $\Delta H_{mf} = 93.1$ J/g is the heat of fusion of fully crystallized PLA [50].

4 Results and Discussion

4.1 Material parameters for the constituents

The geometrical information required by the model includes fiber length L_f and fiber diameter d_f. The statistics of measured L_f and d_f values are 4.71 ± 0.53 mm and 12.50 ± 0.87 μm respectively. The small standard deviations indicate that fiber geometry in the composite is consistent, and thus the averages are used in the model.

Table 1. Parameters of RCF and PLA

Parameter (Unit)	L_f (mm)	d_f (μm)	E_f (GPa)	E_{m1} (GPa)	E_{m2} (GPa)	μ_{m1} (GPa·s)	μ_{m2} (GPa·s)
Values for Figure 4 (a), (c), (d)	4.71	12.50	49.68	8.79	2.46	632.2	8892
Values for Figure 4 (b)	4.71	12.50	39.00	11.00	2.46	700.0	11000

The stress-strain curves of single RCF samples are all approximately linear within the strain of 0.3% (a representative curve given in the supplementary information), which validates the linear elastic assumption of RCF. The measured Young's modulus E_f of the RCF is 49.68 ± 5.06 GPa. In the literature, Zhang et al. [22] reported that the Young's modulus of Lyocell and Viscose fiber bundles at dry state are 8-10 GPa and 3-5 GPa, respectively. To the best of our knowledge, only Cheng et al. [51] evaluated the Young's modulus of single Lyocell fibers using atomic force microscopy and they reported a drastic decrease from 105.2 GPa to 14.1 GPa when the fiber diameter increased from 156 nm to 272 nm. Compared with these works, the BioMid® single fiber has a similar stiffness to that of Lyocell fibers.

A representative strain vs. time curve is shown in the supplementary information for the creep test of pure PLA, i.e., 0.0PLA/RCF. The measured creep compliance, based on five

replicas, is shown by the blue squares in Figure 4 (a). The data exhibits the typical creep behavior of semi-crystalline polymers: an instant elastic compliance followed by a delayed creep compliance (Figure 4 (a)) [37,52]. Equation (4) is used to fit the experimental results of 0.0PLA/RCF and extract the Burgers model parameters of PLA. As shown in Figure 4 (a), a good match is achieved between the experimental data and the model fitting (blue curve), with adjusted $R^2 = 0.99302$. The Burgers model parameters E_1, E_2, μ_1 and μ_2 obtained from the fitting are shown in Table 1, which are close to what was reported in the literature [29,53].

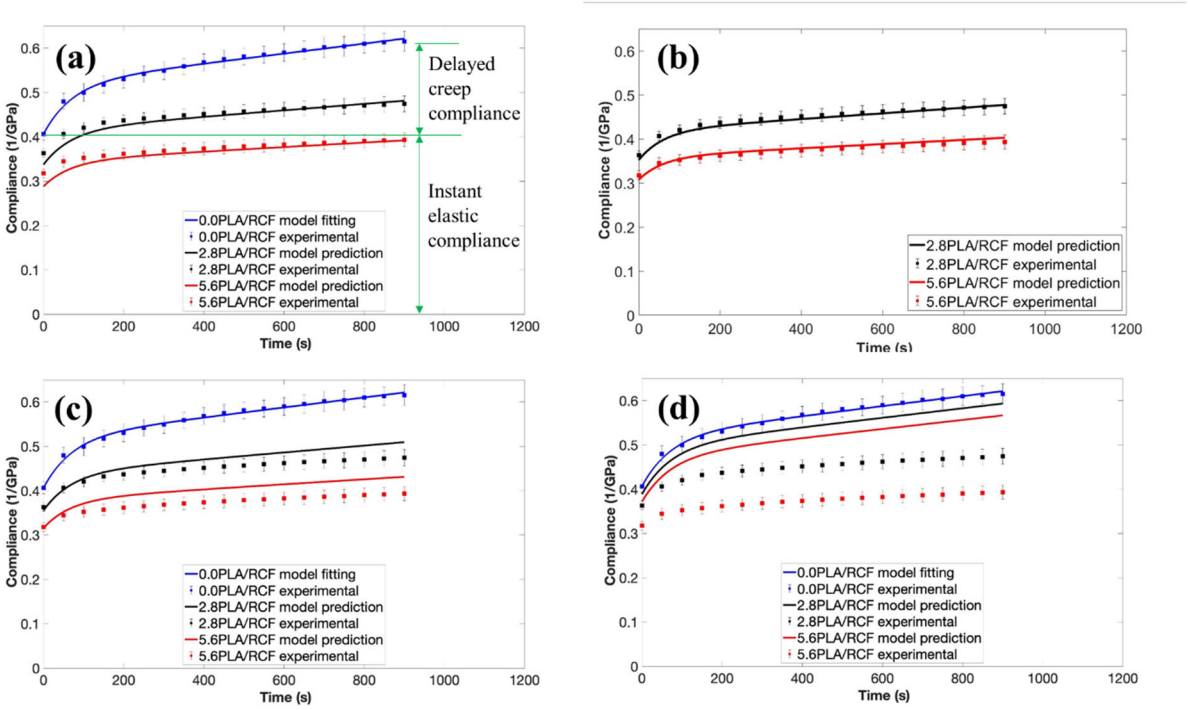

Figure 4. (a) Measured creep compliance and model prediction for PLA and PLA/RCF composites; (b) Demonstration of better comparison with experiments when accounting for increased PLA crystallinity and decreased RCF Young's modulus; (c) Prediction with extended Pan model; (d) Prediction with extended Nielsen model.

4.2 Model prediction for the composites

With the material parameters for the constituents determined, the creep compliance of the PLA/RCF composites can be directly predicted using the developed model. The predicted compliances are plotted in Figure 4 (a) for 2.8PLA/RCF and 5.6PLA/RCF based on equation (14) and the parameters listed in Table 1, with no additional fitting. Comparisons are made in the same figure with experimentally measured compliances (representative strain vs. time curves are provided in the supplementary information), which show good agreement. This confirms that the model developed in this work is capable of predicting the linear viscoelastic behavior of PLA/RCF composites.

From Figure 4 (a), the addition of RCF decreases the instant elastic compliance (Table 2), indicating that the stiffness of the composites (2.8PLA/RCF and 5.6 PLA/RCF) is higher than that of pure PLA (0.0PLA/RCF). There are two potential reasons for the observed increase. Firstly, RCF is significantly stiffer than PLA. The measured Young's modulus of RCF is one order of magnitude larger than the elastic parameters (E_{m1} and E_{m2}) of PLA (see Table 1). Secondly, it has been reported that regenerated cellulose can serve as nucleation agents and increase the crystallinity X_c of PLA [26,54]. As such, higher stiffness was reported for PLA/RCF composites by Suryanegara et al. [55] and Zakir et al. [56], when compared to bare PLA. To confirm this for our study, DSC characterization was conducted and equation (15) was used to determine X_c. As shown in Table 2, X_c of pure PLA is indeed lower than that in the composites, and X_c increases with the RCF concentration. Another observation made from Figure 4 (a) is that the delayed creep compliance decreases with increasing RCF concentration (data summarized in Table 2). In addition to the enhanced elasticity caused by RCF [45,57], hydrogen bonds formed

between PLA and RCF can also lead to extra hinderance that reduces the mobility of PLA chains during creep [57], thereby decreasing the delayed creep compliance.

Table 2. Variation of composite properties with respect to RCF concentration

RCF concentration (wt%)	Crystallinity of PLA matrix (%)	Instant elastic compliance (GPa^{-1})	Delayed creep compliance (GPa^{-1})
0	22.8	0.406	0.209
2.8	25.6	0.363	0.111
5.6	31.9	0.318	0.076

4.3 Discussion

Re-examination of Figure 4 (a) reveals that compared with experimental data for 2.8PLA/RCF and 5.6PLA/RCF, the model slightly underestimated the initial elastic compliance and overestimated the delayed creep compliance. The material parameters used for 2.8PLA/RCF and 5.6PLA/RCF were extracted from pure RCF and PLA without modification, while DSC characterization shows that the crystallinity of PLA was increased by the addition of RCF (Table 2). This might explain the overestimated delayed creep compliance since the additional crystals formed can increase the elasticity as well as providing extra hinderance when polymer chains slip past each other under external load [58]. As a result, the material parameters of PLA (E_{m1}, E_{m2}, μ_{m1} and μ_{m2}) may increase as X_c increases, causing the delayed creep compliance to decrease [58]. For the underestimated instant elastic compliance, we hypothesize that it might be due to the minor amount of moisture absorbed during the creep tests, which were conducted under 22% RH. Rozite et al. [24] discovered that the compliance of PLA/RCF composites increased as the RH level of the testing environment increased from 34% to 66%. The strong hydrophilicity of cellulose makes it susceptible to moisture adsorption. For example, through both experiments and molecular dynamics simulations, Sahputra et al. [59] reported a drastic decrease of cellulose Young's modulus with increasing moisture content. A preliminary test has

been conducted by the authors where the Young's modulus of single RCF samples decreased to around 35 GPa when 4 wt% of moisture was absorbed. To test the above hypotheses, the material parameters in the model were slightly modified, with the PLA parameters increased to reflect the increased crystallinity and the Young's modulus of RCF slightly decreased to capture the effect of absorbed moisture. The model predictions using the revised parameters (listed in Table 1) are given in Figure 4 (b), which shows almost perfect matching with the experimental data. Future work can be done to model the effect of crystallinity change and moisture adsorption more explicitly.

The approach used to extend the Halpin-Tsai-Pagano model into the linear viscoelastic domain can be applied to other linear elastic composite models. Here we demonstrate two other models, namely those by Pan [36] and by Nielsen [60]. Pan [36] derived a modified rule of mixture, given by equation (16), that predicts the Young's modulus of the composites E_c based on the Young's modulus of the fiber E_f, that of the matrix E_m, and fiber volume fraction V_f.

$$E_c = E_f \frac{V_f}{\pi} + E_m(1 - \frac{V_f}{\pi}) \tag{16}$$

Using equation (16) and the correspondence principle, the creep compliances of the PLA/RCF composites are obtained and shown in Figure 4 (c). Compared with the experimental results, within the range of fiber concentration considered in this study, Pan's model can accurately predict the instant elastic compliance but significantly overestimate the delayed creep compliance. To determine the elastic modulus of composites reinforced by uniformly distributed spherical particles, Nielsen [60] modified the Halpin-Tsai equation into

$$\frac{E_c}{E_m} = \frac{1 + (k-1)\eta V_f}{1 - \eta\psi V_f} \tag{17}$$

where

$$\eta = \frac{E_f/E_m - 1}{E_f/E_m + (k-1)}$$
$$\psi = 1 + \frac{V_f^2}{\left(1 - V_f\right)^2} \tag{18}$$

and k is the Einstein coefficient that depends on the Poisson's ratio of the matrix. For the PLA used in this study, Mirkhalaf and Fagerström [61] reported a Poisson's ratio of 0.3, which gives $k = 2.1$ [60]. Extension of Nielsen's model by the correspondence principle leads to a new set of predictions for the composite's creep compliances, which are shown in Figure 4 (d). From the comparison with experiments, Nielsen's model significantly overestimates both the instant elastic compliance and the delayed creep compliance, suggesting the underestimation of the fiber reinforcement effect by the Nielsen's model. One possible explanation is that Nielsen's model was developed for spherical reinforcements instead of short fiber reinforcements. Therefore, the effect of fiber aspect ratio was not considered and could lead to discrepancies between model prediction and experimental results. Comparing all three models, the Halpin-Tsai-Pagano model extended by the correspondence principle offers the best prediction for the creep compliance of PLA/RCF bio-based composites.

5 Conclusion

The Halpin-Tsai-Pagano model for linear elastic composites was extended to the linear viscoelastic regime to describe the mechanical response of PLA/RCF bio-based composites. Based on the correspondence principle, the model only requires information on the constitutive relation of the constituents, concentration of the RCF and geometry of the RCF. Good agreement was found between model prediction and creep compliance measured experimentally for PLA/RCF composites with different RCF concentration. The addition of RCF reduced not only

the instant elastic compliance, but also the delayed creep compliance. The same approach was also applied to extend the linear elastic Pan model and Nielsen model into the linear viscoelastic domain, but the Halpin-Tsai-Pagano model offered the best performance among the three. The model developed in this work has the potential to predict viscoelastic properties of different types of short fiber reinforced bio-based composites.

Supplementary information

The expressions of F_j (j = 0 to 6) and D_k (k = 2 to 7) in equation (13); discussion on fiber orientation in the composite; representative stress and strain curves.

References

[1] A.K. Mohanty, M. Misra, G. Hinrichsen, Biofibres, biodegradable polymers and biocomposites: An overview, Macromol. Mater. Eng. 277 (2000) 1–24.

[2] A.K. Mohanty, M. Misra, L.T. Drzal, Natural fibers, biopolymers, and biocomposites, Taylor & Francis, Boca Raton, 2005.

[3] Georgios Koronis, Arlindo Silva, Green Composites for Automotive Applications, Woodhead Publishing, 2019.

[4] K. Jha, R. Kataria, J. Verma, S. Pradhan, Potential biodegradable matrices and fiber treatment for green composites: A review, AIMS Mater Sci. 6 (2019) 119–138. https://doi.org/10.3934/matersci.2019.1.119.

[5] M. Shibata, S. Oyamada, S.-I. Kobayashi, D. Yaginuma, Mechanical Properties and Biodegradability of Green Composites Based on Biodegradable Polyesters and Lyocell Fabric, J Appl Polym Sci. 92 (2004) 3857–3863.

[6] E. Castro-aguirre, F. Iñiguez-franco, H. Samsudin, X. Fang, R. Auras, Poly (lactic acid) — Mass production , processing , industrial applications , and end of life, Adv. Drug Delivery Rev. . 107 (2016) 333–366. https://doi.org/10.1016/j.addr.2016.03.010.

[7] N. Kurokawa, A. Hotta, Regenerated cellulose nanofibers fabricated through electrospinning and saponification of cellulose acetate as reinforcement of polylactide composites, Cellulose. 26 (2019) 7797–7808. https://doi.org/10.1007/s10570-019-02623-6.

[8] N.F. Zaaba, M. Jaafar, A review on degradation mechanisms of polylactic acid: Hydrolytic, photodegradative, microbial, and enzymatic degradation, Polym. Eng. Sci. 60 (2020) 2061–2075. https://doi.org/10.1002/pen.25511.

[9] G. Rajeshkumar, S. Arvindh Seshadri, G.L. Devnani, M.R. Sanjay, S. Siengchin, J. Prakash Maran, N.A. Al-Dhabi, P. Karuppiah, V.A. Mariadhas, N. Sivarajasekar, A. Ronaldo Anuf, Environment friendly, renewable and sustainable poly lactic acid (PLA) based natural fiber reinforced composites – A comprehensive review, J Clean Prod. 310 (2021) 127483. https://doi.org/10.1016/j.jclepro.2021.127483.

[10] M.A. Sawpan, K.L. Pickering, A. Fernyhough, Hemp Fibre Reinforced Poly(lactic acid) Composites, Adv. Mater. Process. 29–30 (2007) 337–340. http://www.scientific.net/AMR.29-30.337.

[11] B. Baghaei, M. Skrifvars, L. Berglin, Manufacture and characterisation of thermoplastic composites made from PLA/hemp co-wrapped hybrid yarn prepregs, Compos Part A Appl Sci Manuf. 50 (2013) 93–101. https://doi.org/10.1016/j.compositesa.2013.03.012.

[12] L. Suryanegara, A.N. Nakagaito, H. Yano, The effect of crystallization of PLA on the thermal and mechanical properties of microfibrillated cellulose-reinforced PLA composites, Compos Sci Technol. 69 (2009) 1187–1192. https://doi.org/10.1016/j.compscitech.2009.02.022.

[13] R. Auras, L. Lim, SusanE.M. Selke, H. Tsuji, Polylactic Acid, Synthesis, Structures, Properties, Processing, and Applications, John Wiley and Sons, Hoboken, 2010.

[14] A.K. Bledzki, A. Jaszkiewicz, D. Scherzer, Mechanical properties of PLA composites with man-made cellulose and abaca fibres, Compos Part A Appl Sci Manuf. 40 (2009) 404–412. https://doi.org/10.1016/j.compositesa.2009.01.002.

[15] S.H. Lee, S. Wang, Y. Teramoto, Isothermal crystallization behavior of hybrid biocomposite consisting of regenerated cellulose fiber, clay, and poly(lactic acid), J Appl Polym Sci. 108 (2008) 870–875. https://doi.org/10.1002/app.26853.

[16] M.M. Kim, B.S. Kim, J.R. Ha, S.K. Kim, J.W. Yi, J.Y. Lim, Interfacial optimization of lyocell fabric/PLA with silane treatments, Adv Mat Res. 123–125 (2010) 1155–1158. https://doi.org/10.4028/www.scientific.net/amr.123-125.1155.

[17] J.H. Lin, A.P. Chen, J.Y. Lin, T.A. Lin, C.W. Lou, Manufacturing technique and mechanical properties of environment-protective composite nonwoven fabrics, Adv Mat Res. 287–290 (2011) 2673–2676. https://doi.org/10.4028/www.scientific.net/AMR.287-290.2673.

[18] B. Baghaei, M. Skrifvars, M. Rissanen, S.K. Ramamoorthy, Mechanical and thermal characterization of compression moulded polylactic acid natural fiber composites

reinforced with hemp and lyocell fibers, J Appl Polym Sci. 131 (2014). https://doi.org/10.1002/app.40534.

[19] B. Baghaei, M. Skrifvars, Characterisation of polylactic acid biocomposites made from prepregs composed of woven polylactic acid/hemp-Lyocell hybrid yarn fabrics, Compos Part A Appl Sci Manuf. 81 (2016) 139–144. https://doi.org/10.1016/j.compositesa.2015.10.042.

[20] J.W. Park, T.H. Lee, J.H. Back, S.W. Jang, H.J. Kim, M. Skrifvars, Phenyl silane treatment and carding process to improve the mechanical, thermal, and water-absorption properties of regenerated cellulose lyocell/polylactic acid bio-composites, Compos B Eng. 167 (2019) 387–395. https://doi.org/10.1016/j.compositesb.2019.02.064.

[21] Calvin Woodings, Regenerated cellulose fibers, CRC Press LLC, Boca Raton, 2001.

[22] S. Zhang, C. Chen, C. Duan, H. Hu, H. Li, J. Li, Y. Liu, X. Ma, J. Stavik, Y. Ni, Regenerated Cellulose by the Lyocell Process, a Brief Review of the Process and Properties, Bioresources. 13 (2018) 4577–4592.

[23] M.S. Huda, A.K. Mohanty, L.T. Drzal, E. Schut, M. Misra, “Green” composites from recycled cellulose and poly(lactic acid): Physico-mechanical and morphological properties evaluation, J Mater Sci. 40 (2005) 4221–4229.

[24] L. Rozite, J. Varna, R. Joffe, A. Pupurs, Nonlinear behavior of PLA and lignin-based flax composites subjected to tensile loading, Journal of Thermoplastic Composite Materials. 26 (2013) 476–496. https://doi.org/10.1177/0892705711425846.

[25] B. Bax, J. Müssig, Impact and tensile properties of PLA/Cordenka and PLA/flax composites, Compos Sci Technol. 68 (2008) 1601–1607. https://doi.org/10.1016/j.compscitech.2008.01.004.

[26] Y. Zhang, Y. Jiang, L. Han, B. Wang, H. Xu, Y. Zhong, L. Zhang, Z. Mao, X. Sui, Biodegradable regenerated cellulose-dispersed composites with improved properties via a pickering emulsion process, Carbohydr Polym. 179 (2018) 86–92. https://doi.org/10.1016/j.carbpol.2017.09.065.

[27] J. Ganster, H.P. Fink, Novel cellulose fibre reinforced thermoplastic materials, Cellulose. 13 (2006) 271–280. https://doi.org/10.1007/s10570-005-9045-9.

[28] A. Karakoç, A. Miettinen, J. Virkajärvi, R. Joffe, Effective elastic properties of biocomposites using 3D computational homogenization and X-ray microcomputed tomography, Compos Struct. 273 (2021). https://doi.org/10.1016/j.compstruct.2021.114302.

[29] Y. Chen, T. Tang, C. Ayranci, Moisture-induced anti-plasticization of polylactic acid: Experiments and modeling, J Appl Polym Sci. 139 (2022). https://doi.org/10.1002/app.52369.

[30] R.A. Schapery, Viscoelastic Behavior and Analysis of Composite Materials, in: G.P. Sendeckyj (Ed.), Mechanics of Composite Materials, 1st ed., Academic Press, New York, 1974: pp. 85–168.

[31] A.K. Kaw, Mechanics of Composite Materials, 2nd ed., CRC Press, Boca Raton, 2006.

[32] F. Vilaseca, R. del Rey, R. Serrat, J. Alba, P. Mutje, F.X. Espinach, Macro and micro-mechanics behavior of stifness in alkaline treated hemp core fibres polypropylene-based composites, Compos B Eng. 144 (2018) 118–125. https://doi.org/10.1016/j.compositesb.2018.02.029.

[33] S.W. Tsai, N.J. Pagano, Invarient Properties of Composite Materials, 1968.

[34] J.C. Halpin, J.L. Kardos, The Halpin-Tsai Equations: A Review, Polym Eng Sci. 16 (1976) 345–352.

[35] V. Mazzanti, R. Pariante, A. Bonanno, O. Ruiz de Ballesteros, F. Mollica, G. Filippone, Reinforcing mechanisms of natural fibers in green composites: Role of fibers morphology in a PLA/hemp model system, Compos Sci Technol. 180 (2019) 51–59. https://doi.org/10.1016/j.compscitech.2019.05.015.

[36] N. Pan, The Elastic Constants of Randomly Oriented Fiber Composites: A New Approach to Prediction, Science and Engineering of Composite Materials. 5 (1996) 63–72.

[37] R.M. Christensen, Theory of Viscoelasticity, An Introduction, 2nd ed., Dover Publications Inc., New York, 2003.

[38] W.N. Findley, Creep and relaxation of nonlinear viscoelastic materials : with an introduction to linear viscoelasticity, Dover Publications Inc., New York, 1989.

[39] G. Jiang, W. Huang, L. Li, X. Wang, F. Pang, Y. Zhang, H. Wang, Structure and properties of regenerated cellulose fibers from different technology processes, Carbohydr Polym. 87 (2012) 2012–2018. https://doi.org/10.1016/j.carbpol.2011.10.022.

[40] Z. Hashin, Complex moduli of viscoelastic composites-II. Fiber reinforced materials, Int J Solids Struct. 6 (1970) 797–807. https://doi.org/10.1016/0020-7683(70)90018-1.

[41] B. Raju, S.R. Hiremath, D. Roy Mahapatra, A review of micromechanics based models for effective elastic properties of reinforced polymer matrix composites, Compos Struct. 204 (2018) 607–619. https://doi.org/10.1016/j.compstruct.2018.07.125.

[42] J.C. Halpin, Primer on Composite Materials Analysis, 1st ed., CRC Press, Boca Raton, 1992.

[43] E.H. Backes, L. de N. Pires, L.C. Costa, F.R. Passador, L.A. Pessan, Analysis of the degradation during melt processing of pla/biosilicate® composites, Journal of Composites Science. 3 (2019) 52.

[44] How is BioMid fiber made, (2018). https://biomidfiber.com/ (accessed August 30, 2022).

[45] I.I. Qamhia, Experimental and Analytical Characterization of Regenerated/nano Cellulose Composites, University of Wisconsin-Milwaukee, 2014. http://dc.uwm.edu/etd.

[46] M. Legault, Bio-composites update: Beyong eco-branding, Composites World. (2013). https://www.compositesworld.com/articles/biocomposites-update-beyond-eco-branding (accessed August 30, 2022).

[47] ASTM D3379-75 Standard Test Method for Tensile Strength and Young's Modulus for High-Modulus Single-Filament Materials, 1989.

[48] ASTM D2990-17 Standard Test Methods for Tensile, Compressive, and Flexureal Creep and Creep-Rupture of Plastics, 2017.

[49] L. Lim, R. Auras, M. Rubino, Processing technologies for poly (lactic acid), Prog Polym Sci. 33 (2008) 820–852. https://doi.org/10.1016/j.progpolymsci.2008.05.004.

[50] Fisher EW, Sterzel HJ, Wegner G, Investigation of the structure of solution grown crystals of lactide copolymers by means of chemical reactions, Kolloid-Zeitschrift Und Zeitschrift Für Polymere. (1973) 980–990.

[51] Q. Cheng, S. Wang, D.P. Harper, Effects of process and source on elastic modulus of single cellulose fibrils evaluated by atomic force microscopy, Compos Part A Appl Sci Manuf. 40 (2009) 583–588. https://doi.org/10.1016/j.compositesa.2009.02.011.

[52] M.T. Shaw, W.J. MacKnight, Introduction to Polymer Viscoelasticity, 3rd ed., John Wiley & Sons, Inc., Hoboken, 2005.

[53] I. Widiastuti, I. Sbarski, S.H. Masood, Mechanical behavior of a fluid-sensitive material during liquid diffusion, Mech Time Depend Mater. 18 (2014) 387–406. https://doi.org/10.1007/s11043-014-9233-9.

[54] A. Pei, Q. Zhou, L.A. Berglund, Functionalized cellulose nanocrystals as biobased nucleation agents in poly(l-lactide) (PLLA) - Crystallization and mechanical property effects, Compos Sci Technol. 70 (2010) 815–821. https://doi.org/10.1016/j.compscitech.2010.01.018.

[55] L. Suryanegara, A.N. Nakagaito, H. Yano, Thermo-mechanical properties of microfibrillated cellulose-reinforced partially crystallized PLA composites, Cellulose. 17 (2010) 771–778. https://doi.org/10.1007/s10570-010-9419-5.

[56] K.M. Zakir, A.J. Parsons, C.D. Rudd, I. Ahmed, W. Thielemans, Mechanical , crystallisation and moisture absorption properties of melt drawn polylactic acid fibres, Eur Polym J. 53 (2014) 270–281. https://doi.org/10.1016/j.eurpolymj.2014.02.001.

[57] M.S. Huda, L.T. Drzal, A.K. Mohanty, M. Misra, Chopped glass and recycled newspaper as reinforcement fibers in injection molded poly(lactic acid) (PLA) composites: A comparative study, Compos Sci Technol. 66 (2006) 1813–1824. https://doi.org/10.1016/j.compscitech.2005.10.015.

[58] L.H. Sperling, Introduction to Physical Polymer Science, John Wiley & Sons, Inc, 2006.

[59] I.H. Sahputra, A. Alexiadis, M.J. Adams, Effects of Moisture on the Mechanical Properties of Microcrystalline Cellulose and the Mobility of the Water Molecules as Studied by the Hybrid Molecular Mechanics–Molecular Dynamics Simulation Method, J Polym Sci B Polym Phys. 57 (2019) 454–464. https://doi.org/10.1002/polb.24801.

[60] L.E. Nielsen, Generalized equation for the elastic moduli of composite materials, J Appl Phys. 41 (1970) 4626–4627. https://doi.org/10.1063/1.1658506.

[61] S.M. Mirkhalaf, M. Fagerström, The mechanical behavior of polylactic acid (PLA) films: fabrication, experiments and modelling, Mech Time Depend Mater. (2019). https://doi.org/10.1007/s11043-019-09429-w.